Mon. Not. R. Astron. Soc. **000**, 1–9 (2005) Printed 1st September 2005 (MN LATEX style file v2.2)

Formation of H-α from classical T Tauri stars: the disc, wind, and magnetospheric-accretion hybrid model

Ryuichi Kurosawa⋆, Tim J. Harries and Neil H. Symington
School of Physics, University of Exeter, Stocker Road, Exeter EX4 4QL

Dates to be inserted

ABSTRACT

We investigate the formation of Hα from classical T Tauri stars with a complex circumstellar geometry – the combination of mangnetisherical accretion, out-flowing jet/stellar wind, and accretion disc. AND MORE

Key words: stars:formation – stars: individual: SU Aur – circumstellar matter – infrared: stars – stars: pre-main-sequence

1 INTRODUCTION

T Tauri stars (TTS) are young ($<\sim 3\times10^6\,\mathrm{yrs}$, Appenzeller & Mundt 1989) low-mass stars, and known as progenitors of solar-type stars. Classical T Tauri stars (CTTS) exhibit strong Hα emission, and typically have spectral types of F–K. Some of the most active CTTS show emission in higher Balmer lines and metal lines (e.g., Ca II H and K). They also exhibit an excess amount of continuum flux in the ultraviolet (UV) and infrared (IR). Their spectral energy distribution and polarization data suggest the presence of a circumstellar disc, and it plays an important role in regulating dynamics of gas flows around CTTS.

Many observational studies (e.g., Herbig 1962; Edwards et al. 1994; Kenyon et al. 1994; Reipurth et al. 1996; Alencar & Basri 2000) of CTTS line profles show that the evidence for both outward wind/jet flows and inward accretion flows, as seen in the blueshifted absorption features in Hα profiles and the redshifted inverse P Cygni (IPC) profiles. Typical mass-loss rates of CTTS are about $10^{-9}\,\mathrm{M_\odot\,yr^{-1}}$ to $10^{-7}\,\mathrm{M_\odot\,yr^{-1}}$ (e.g., Kuhi 1964; Edwards et al. 1987; Hartigan et al. 1995), and the mass-accretion rates are also about $10^{-9}\,\mathrm{M_\odot\,yr^{-1}}$ to $10^{-7}\,\mathrm{M_\odot\,yr^{-1}}$ (e.g., Kenyon & Hartmann 1987; Bertout, Basri, & Bouvier 1988; Gullbring et al. 1998).

Recent Hα spectro-astrometric observations by Takami et al. (2003) show the direct evidence for the presence of bipolar and monopolar outflows down to $\sim$ 1 AU scale (e.g. CS Cha and RU Lup). Similarly, ESO VLT observation of high-resolution ($\mathrm{R}=50\,000$) two-dimensional spectral of edge-on CTTS (HH30*, HK Tau B, and HV Tau C) by Appenzeller et al. (2005) show the extended (SCALE?) Hα emission in the direction perpendicular to the obscuring circumstellar disc, and in both above and below the disc — suggesting the presence of the bipolar outflows. In silightly larger scale, *HST* observation of HH30 (Burrorws et al 1996) shows the jet traced to within $\lesssim$ 30 AU from the star. The jet has a cone shape with an opening angle of 3° between 70 and 700 AU. (Originally from Konig and Pudritz 2000 review in PP IV). Alencar & Basri 2000 found about 80 per cent of their samples (30 CTTS) show blueshifted absorption componets in at least one of Balmer lines and Ca K (most commonly in Hα).

In a currently favoured model of accretion flows around CTTS, the accretion discs are disrupted by the magnetosphere of stars which channels the gas from the disc onto the surface of the stars (e.g., Uchida & Shibata 1985; Königl 1991; Collier Cameron & Campbell 1993Shu et al. 1994). This picture of the accretion flows is supported by the evidences that CTTS have relatively strong ($\sim 10^3\mathrm{G}$) magnetic field (e.g., Johns-Krull, Valenti, Hatzes, & Kanaan 1999; Guenther & Emerson 1996) and by the radiative transfer models which reproduce the observed profiles for some TTS (Muzerolle et al. 2001). The magnetospherical accretion model naturally explains the blueward asymmetic emission lines (seen in some of CTTS) caused by the partial occulation of the flow by the disc, and the redshifted absorption componet at the typical free-fall velocities (a few hundred $\mathrm{km\,s^{-1}}$) seen in some of CTTS.

Dispite the success of the magnetosherical accretion model in explaining the line profiles in some CTTS, the overwhelming observational evidences for the outflow (mentoned above) in the CTTS profiles suggests that this model is only a part of a whole picture. Clearly, the modefification to include the outflowing wind/jet flow is neccessary if one requires to predict the mass-accretion rate and the mass-loss rate of CTTS by modelling their emission profiles (e.g. Hα).

Priory to the magnetospherical models, many alternative models had been considered to explain the observed spectroscopic features mentioned earlier. For example, 1. the Alfvén wave-driven wind model (e.g. Decampli 1981; Hartmann et al. 1982), 2. turbulant boundary layer (between the accretion disc and stellar surface) model (e.g. Bertout et al. 1988; Basri & Bertout 1989), 3. chromospheric model (e.g. Calvet et al. 1984), and 4. disc wind model (e.g. Calvet et al. 1992; Kwan & Tademaru 1995). Considering the sucess of the magnetospherical accretion flow model in

⋆ E-mail: rk@astro.ex.ac.uk

some cases and the observational eividences for the outflows, it is likely that an improved spectroscopic model requires both inflow and outflow components. The combination of the magnetospheric accretion flow model with model 1 or 4 would be a reasonable starting point for an improved spectroscopic model. Although time consuming to explore a larger parameter space, more realistic density, velocity and temperature structure from magnetohydrodynamic wind+accretion models should be considered as inputs for an radiative transfer model in the future.

The magnetocentrifugal wind model, first proposed by Blandford & Payne (1982), has been often used to reproduce the large-scale wind structure of T Tauri stars, or to model observed optical jets (e.g. HH 30 jet by Burrows et al. 1996; Ray et al. 1996). The lanching of the wind from a Keplerian disc is typically done by treating the equaotorial plane of the disc as a mass-injecting boundary condition (e.g., Ustyugova et al. 1995; **?**); Ouyed & Pudritz 1997; Krasnopolsky et al. 2003). Depending on the location of the open magnetic fields anchored to the disc, two different types of winds are preoduced. If the field is constrained to be near the corotation radius of stellar magnetosphere, an "X-wind" (Shu et al. 1994) is produces. If the open field lines are located in a wider area of the disc, a "disc-wind" similar to Königl & Pudritz (2000) is produced Krasnopolsky et al. (2003). Recent reviews on the jet/wind-disc connection can be found in Königl & Pudritz (2000) and Pudritz & Banerjee (2005).

In this paper, we present a wind/jet – accretion disc – magnetospherical accretion hybrid model for CTTS, and study the formation of Hα to understand the wide varaiety emission line profiles seen in the observation. Using the model results, we examine the Hα spectroscopic classification used by Reipurth et al. (1996), and discuss the basic physical conditions required to reproduce Hα profiles from each of their classified types. We also examine whether the Hα models are consistent with some predictions made by the recentt MHD studies (e.g. $\mu = \dot{M}_{\rm wind}/\dot{M}_{\rm acc} \approx 0.1$).

In section 2, the model assumptions, and the basic model configurations are presented. We discuss the radiaive transfer model used to compute the profiles in section 3, and the results of model calculations are given in section 4. The closer examination and discussion of the results are presented in section 5. Finally, the summary of this work and the conclusion are in section 6.

2 MODEL CONFIGURATION

To understand how the different part of the CTTS circumsterllar enviroment contributes to the fomation of Hα, the model spaced is devided into four different regions: 1. Central contiuum source, 2. magnetosphere accretion flow, 3. wind/Jet outflow, and 4. accretion disc. Fig. 1 depicts the relative location in the model space. In all regions, the density is symmetric around the z-axis. The innermost raius of the magnetsphere at the equotrial plane coincides with the the inner radius of the accretion disc. From the inner most part of the accretion disc, the gas freely fall, moving along the magneic filed onto the surface of the star. For the purpose of computational simplicity, the colliminated wind/jet are defined only in the outside of the largest radius of the magnesophere. In the following subsections, the details of model components will be described.

2.1 Contiuum Source

Unless specified otherwise, we adopt stellar parameters of a typical classical T Tauri star (REF) for the central conitnuum source, i.e. radius (R_*), mass (M_*), and effective temperature the photosphere ($T_{\rm ph}$) are $2\,R_\odot$, $0.5\,M_\odot$, and $4000\,{\rm K}$ respectively. The model atomsphere of Kurucz (1979) equivallently Kurucz (1993) with $T_{\rm ph} = 4000\,{\rm K}$ and $\log g_* = 3.5$ (cgs) is used to continuum flux at Hαwavelength. The parameters are summarised in Table 1.

The limb-darkening law used for the continuum source is $I(\mu) = I_0\,(1 + b\mu)$ where $\mu = \cos\theta$ and θ is the polar angle. b is a parameter. For no limb-darkening case, $b = 0$, and for the Eddington approximation case $b = 3/2$. The former is used in all the calulcations presented here. (Is this an ok assumption for T Tauri's? You need to check this.)

2.2 Magnetosphere

We adopt the magnetospherical accretion flow model of Hartmann et al. (1994), as done so by Muzerolle et al. (2001) and by Symington et al. (2005), in which the gas accretion on to the stellar surface from the innermost part of the accretion disc occurs through a dipolar stellar magnetic field. The magnetic field is assumed to be so strong that the gas flow does not affect the underlying magnetic field itself. As shown in Fig. 1, the innermost radius ($R_{\rm mi}$) of the magnetophere at the equatorial plane ($z = 0$) is assigned to be same as the inner radius ($R_{\rm di}$) of the accretion disc where the flow is truncated. In our models, $R_{\rm mi}$ and the outer radius ($R_{\rm mo}$) of the magnetosphere (at the equaotrial plane) are set to be $2.2\,R_\odot$ and $3.0\,R_\odot$ respectively. The former value corresponds to the corotation radius of the accretion disc, and the geometry of the magnetic field/stream lines is kept constant throghout this paper. The geometry of the magnetosphere is identical to the "small/wide" model of Muzerolle et al. (2001).

The magnetic field and the gas stream lines are assumed to have the following simple form: $r = R_{\rm m}\sin^2\theta$ (see Ghosh et al. 1977) where r, and θ are coordinates of the field point (p) in Fig. 1 in spheical coodinates, and $R_{\rm m}$is the radial distance to the field line at the equotorial plane ($\theta = \pi/2$). The range of $R_{\rm m}$is restricted between $R_{\rm mi}$ and $R_{\rm mo}$ as mentioned above. Using the field geometry above, the conservation of energy, and igoring the rotation of magnetosphere, the velocity and the density of the accreting gas along the steam line can be found. See Hartmann et al. (1994) for details.

In all of our models, the temperature structure of the magnetospheric used by Hartmann et al. (1994) is also adoped here. The temperature structure was computed assuming a volumetric heating rate which is proportional to r^{-3}, and using the energy balance of the radiative cooling rate of Hartmann et al. (1982) and the heating rate (Hartmann et al. 1994). Although the temperature structure of the accretion steam could significantly affect the line source function, for the purpose of the expolaring the general characteristics of the Hα formation, this simple form is a reasonable assumption.Martin (1996) presented the self-consistent determination of the thermal structure of the inflowing gas along the dipole magnetic field, same as the one used here, by solving the heat equation couple to trate equations for hydrogen. He found that main heat source is adiabatic compression due to the convering nature of the flow, and the major contirbutors of the cooling process are bremsstrahling radiation and line emission from Ca II and Mg II ions. The temerature sturcture of Martin (1996) qualitaively agrees with that of (Hartmann et al. 1994). The sensitivty tests of Hα on the temperature structure will be presented later (SPECIFY THE SECTION LATER).

As the infalling gas becomes closer to the stellar surface, it is decelerates in a strong shock, and heated to $\sim 10^6\,{\rm K}$ (with typical parameters). The X-ray radiation produced in the shock will

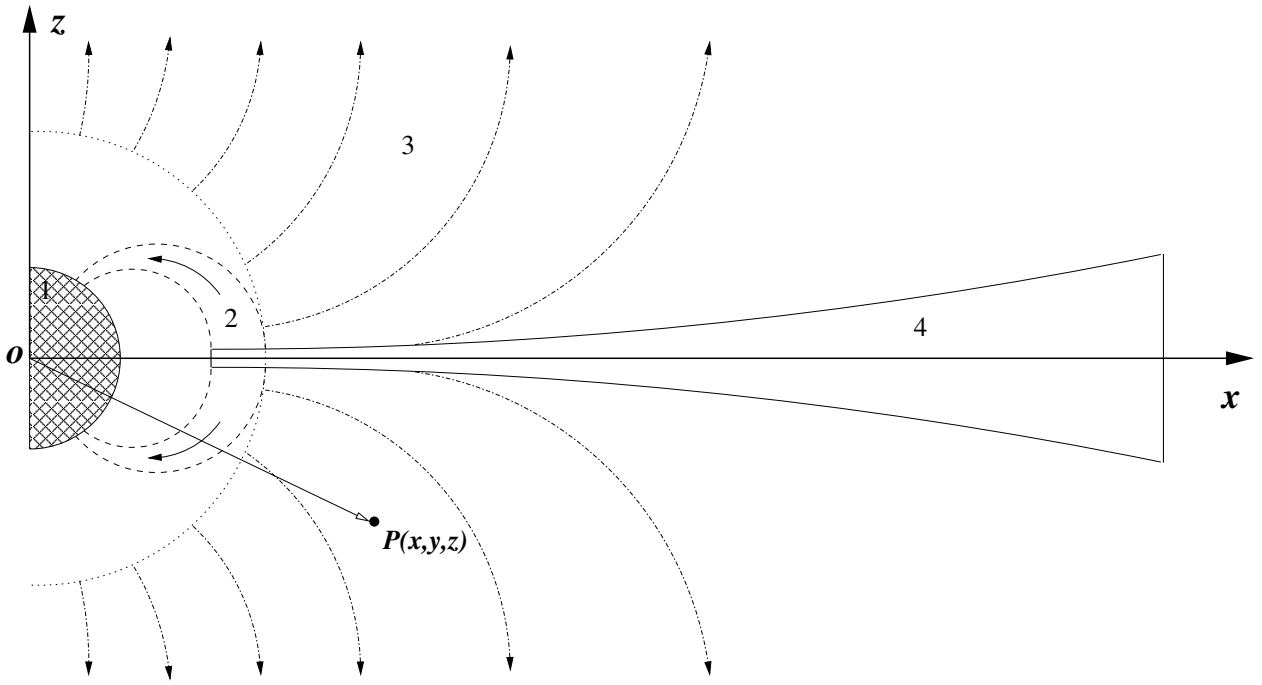

Figure 1. Basic Model Configuration. The system consist of four components: 1. the continuum source located at the origin (o) of the cartisian coordinates (x, y, z) – the y-axis are into the paper, 2. magnetospherical accretion flow, 3. colliminated wind/jet outflow, and 4. accretion disc. The density distribution is symmetric around the z-axis. The innermost raius of the magnetsphere (at the equotrial plane) coincides with the the inner radius of the accretion disc. From the inner most part of the accretion disc, the gas freely fall, moving along the magneic filed onto the surface of the star. For simplicit, the colliminated wind/jet exists outside of the largest radius of the magnesophere (dotted line).

Parameters	R_* $[R_\odot]$	M_* $[M_\odot]$	$T_{\rm ph}$ [K]	$R_{\rm mi}$ $[R_*]$	$R_{\rm mo}$ $[R_*]$	$\dot{M}_{\rm acc}$ $[M_\odot\,{\rm yr}^{-1}]$	$\dot{M}_{\rm wind}$ $[M_\odot\,{\rm yr}^{-1}]$	β $[-]$	v_∞ $[{\rm km\,s}^{-1}]$	m $[-]$	$R_{\rm di}$ $[R_\odot]$	$R_{\rm do}$ [AU]
Standard	2.0	0.5	4000	2.2	3.0	10^{-7}	10^{-8}	0.2	200	2.0	2.0	100

Table 1. The summary of the standard classical T Tauri star model parameters.

be absorbed by the gas located near, and reemitted in optical and UV radiation (Königl 1991; Hartmann et al. 1994). This will create hot rings near the stellar surface where the magnetic field intersects with the surface. For simplicity, the free-falling kinetic energy is assumed to be thermalized in the radiating layer, and reemits as blackbody radiation (with a single temerature). With the parameters of the magnetosphere and the star given above (Table 1), about 8 per cent of the surface is covered by the hot rings, and its temperature is about 6400 K. If the mass-accretion rate is $10^{-7}\,{\rm M}_\odot\,{\rm yr}^{-1}$, the ratio of this accretion luminosity to the photospheric luminosity is about 0.5. The contiuum emission from the hot rings is taken into account when computing the line profiles.

2.3 Wind/Jet

2.3.1 Colliminated wind model

JUSTTIFICATION OF USING THIS FORMULATION. BREIFLY MENTIONED THE WORK DONE BY OTHERS.

Based on the simple model of Appenzeller et al. (2005), the following parametrisation of colliminated wind/jet (region 3 in Fig. 1) is adopeted. The wind velocity field, $\mathbf{v}_{\rm wind}\,(r,\theta)$, is consist of radial and polar components which depend only on r and θ respectively. The radial componet $v_r\,(r)$ is assumed to be in the classical beta-velocity law (c.f. Castor & Lamers 1979), and the azimuthal component v_ϕ is asuumed to be a constant fraction (γ) of the Keplerian velocity for a given distance $(w = \sqrt{x^2+y^2})$ from the symmetry axis (z-axis) , i.e.:

$$\mathbf{v}_{\rm wind} \;=\; v_r\hat{\mathbf{r}} + v_\phi\hat{\boldsymbol{\phi}} + v_\theta\hat{\boldsymbol{\theta}} \tag{1}$$

where

$$v_r\,(r) = v_{r0} + v_\infty\left(1-\frac{R_{\rm mo}}{r}\right)^\beta\,, \tag{2}$$

$$v_\phi\,(w) = \gamma\left(\frac{GM_*}{w}\right)^{1/2}\,, \tag{3}$$

and

$$v_\theta\,(r,\theta) = v_{\theta 0}\left(\frac{R_{\rm mo}}{r}\right)^\alpha\frac{\tan\theta}{|\tan\theta|}\,. \tag{4}$$

Note that the base of the wind starts at $r = R_{\rm mo}$, and the range of the polar angle is restricted to $\theta > |\theta_{\rm disc}|$ where $\theta_{\rm disc}$ is the openning angle of the accretion disc, to avoid the overlap. $v_{r0}$is the small radial velocity at the base of the wind ($r = R_{\rm mo}$). Normally,

$v_{r0} = 10\,\mathrm{km\,s^{-1}}$, approximately the thermal velocity of hydrogen with $T = 7500\,\mathrm{K}$ and $\gamma = 0.05$ (Appenzeller et al. 2005) are used. The dependency of v_r in polar direction ($\theta = 0$) on the values of wind accerelation parameter β is shown in Figure 2. All other parameters describing the wind are fixed as the standard values given in Table 1.

Further, the density of the wind is assumed to be axisymmetric and separable in r and θ for computationaly simpliciy, i.e.,

$$\rho\left(r,\theta\right) = P\left(r\right)\ F\left(\theta\right) \tag{5}$$

with

$$F\left(\theta\right) = n\ \cos^{b}\theta \tag{6}$$

where b is normally positive even number (for the density symmetric about the equtotrial plane), and n is the angular normalisation constant. For $b = 0$, the wind is sherically symmetic exept for the parts dirupted by the accretion disc. The larger the value of b, the higher the degree of the collimination. By integrating equation 6 over angles and normalising the integral to 4π, one finds

$$n = \frac{1+b}{1-\cos^{1+b}\theta_{\mathrm{wind}}}\,. \tag{7}$$

Asumming the total mass-loss rate by the wind/jet is $\dot{M}_{\mathrm{wind}}$ and the mass-flux conserves in time, the radial part of the density function is reduced to $P\left(r\right) = \dot{M}_{\mathrm{wind}}\ \left[4\pi r^2 v_r\left(r\right)\right]^{-1}$; hence, Equation 5 becomes

$$\rho\left(r,\theta\right) = \frac{n\ \cos^{b}\theta\,\dot{M}_{\mathrm{wind}}}{4\pi r^2\,v_r\left(r\right)}\,. \tag{8}$$

For a given mass-accretion rate, the wind mass-loss rate in our typical model is assined from the ratio of mass-loss to mass-accretion rate ($\dot{M}_{\mathrm{wind}}/\dot{M}_{\mathrm{acc}} \approx 0.1$), indicated by both observations and magnetohydrodynamical calculations (see e.g. Königl & Pudritz 2000).

Figure 2 shows the values of ρ in polar direction ($\theta = 0$) for different values of β with all other parameters fixed as the standard values (Table 1).

2.3.2 *Disc-wind model*

GIVE MORE CONVINCING MOTIVIATION FOR USING THIS MODEL. THIS SECTION MAY BE DELETED.

Alternative to the colliminated wind model, the kinematic disc-wind mode of Knigge et al. (1995) in which a wind originating from the surface of the accretion disc with a biconical outflow geometry (Fig. XXX) will be presented next. The model was originally developed for describing the formation of the UV resonance lines in the winds of cataclystic variable (CV) stars.

2.4 Accretion disc

Region 4 in Fig. 1

2.4.1 *Density and velocity*

Although it is possible, in our model, to compute the vertical hydrostatic structure of the accretion disc self-consistently (assuming the radial dependecy of the mid-plane density) by using the interative Monte Calro radative transfer technique of Walker et al. (2004), we find it to be too time consuming for the purpose of this paper – understanding the general characteristic of Hα profile shapes hence exploring a large parameter space. For this reason, we adopt a simple analytical disc model, the steady α-disc 'standard model' (Shakura & Sunyaev 1973; Frank, King, & Raine 2002) for the disc density disribution, i.e.

$$\rho_{\mathrm{d}}\left(w,z\right) = \Sigma\left(w\right)\ \frac{1}{\sqrt{2\pi}h\left(w\right)}e^{-\left(\frac{z}{2h\left(w\right)}\right)^2} \tag{9}$$

where w, h, z and Σ are the distance from the symmetry axis, the scale height, the distance from the disc plane, and the surface density at the mid-plane, respectively. The mid-plane surface density and the scale height are given as:

$$\Sigma\left(w\right) = \frac{5M_{\mathrm{d}}}{8\pi R_{\mathrm{d}}^2}\,w^{-3/4} \tag{10}$$

where R_{do} and M_{d} are the disc radius and the disc mass respectively.

$$h\left(w\right) = 0.05\,R_{\mathrm{do}}\,w^{9/8}\,. \tag{11}$$

With these parameters, the disc is slightly flared. The inner radius of the disc is set to $R_{\mathrm{di}} = R_{\mathrm{mi}}$ (the inner radius of the magnetosphere at the equaotrial plane), which is approximatly same as the co-rotating radius of the system with the paramters in Table 1. The disc mass, M_{d}, of an object is assumed to be 1/100 of the central mass (M_*), and the disc radius (R_{di}) to be 100 au. The velocity of the gas/dust in the disc is assumed to be Keplerian.

2.4.2 *Dust model*

To calculate the dust scattering and absorption cross section as a function of wavelength, the optical constants of Draine & Lee (1984) for amorphous carbon grains and Hanner (1988) for silicate grains are used. The model uses the "large grain" dust model of Wood et al. (2002) in which the dust grain size distribution is described by the following function:

$$n\left(a\right)da = \left(C_{\mathrm{C}} + C_{\mathrm{Si}}\right)\ a^{-p}\exp\left[-\left(\frac{a}{a_c}\right)^{q}\right]da \tag{12}$$

where a is the grain size restricted between a_{min} and a_{max}, and C_{C} and C_{Si} are the terms set by requiring the grains to completely deplete a solar abundance carbon and silicon. The parameters adopted in our model are: $C_{\mathrm{C}} = 1.32\times10^{-17}$, $C_{\mathrm{Si}} = 1.05\times10^{-17}$, $p = 3.0$, $q = 0.6$, $a_{\mathrm{min}} = 0.1\,\mu$m, $a_{\mathrm{max}} = 1000\,\mu$m, and $a_c = 50\,\mu$m. This corresponds to Model 1 of the dust model used by Wood et al. (2002). See also their Fig. 3 The relative number of each grain is assumed to be that of solar abundance, C/H$\sim\ 3.5\times10^{-4}$ (Anders & Grevesse 1989) and Si/H$\sim 3.6\times10^{-5}$ (Grevesse & Noels 1993) which are similar to values found in the ISM model of Mathis et al. (1977) and Kim, Martin, & Hendry (1994). Similar abundances were used in the circumstellar disc models of Cotera et al. (2001).

3 RADIATIVE TRANSFER MODEL

We have extended the TORUS radiative transfer code (Harries 2000; Kurosawa et al. 2004; Symington et al. 2005) to compute the Hα profiles from pre-main-sequence stars which are surrounded by one or more of the followings: the magnetospherical accretion flow (REF), the out-flowing colliminated wind/jet (REF), and the accreation disc (REF). Previously in Symington et al. (2005), the

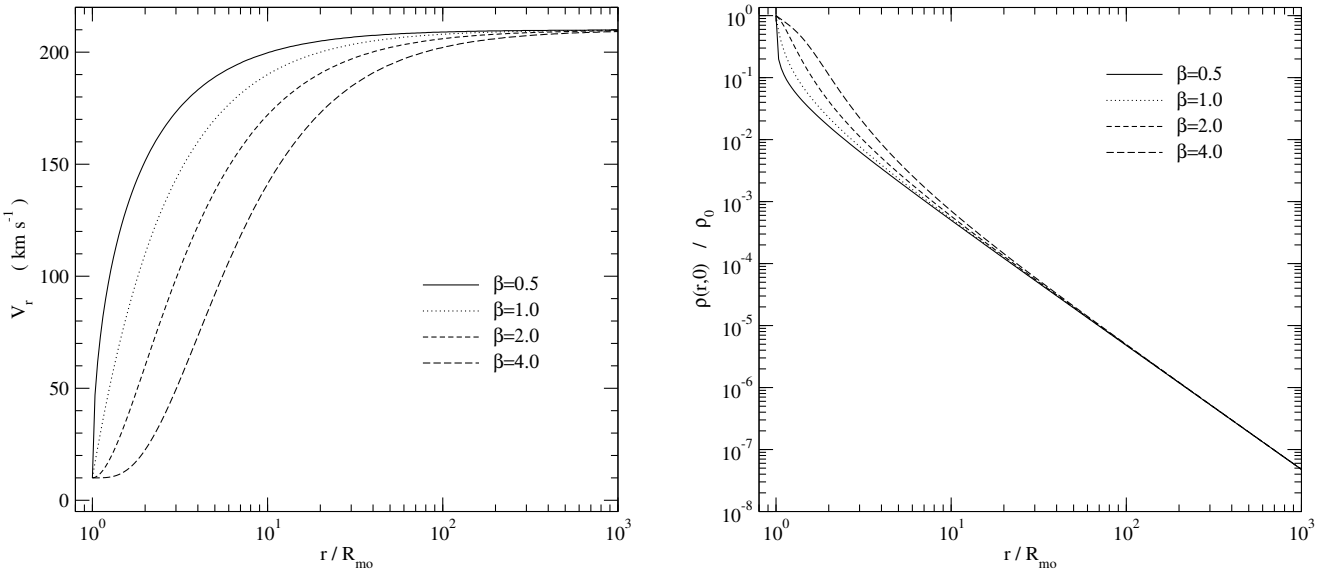

Figure 2. The dependency of the wind/jet velocity and density structures on the wind accerelation parameter β. The radial component of the wind/jet velocity (equation 2) in polar direction, $\theta = 0$ as a function of radius is shown on left. The wind/jet density (equation 8 along polar direction as a function of radius is right. The smaller the value of β, the faster the accerelation of the wind. For the raidus ($r/R_{\rm mo} < 10$, both velocity and density are sensitive to the value of β. For all β values, the radial velocity of the wind reaches the terminal velocity ($\sim 210\,{\rm km\,s^{-1}}$ by $r/R_{\rm mo} \sim 1000$. The initial velocity $V_0 = 10\,{\rm km\,s^{-1}}$, which approximately corresponds to the thermal velocity of a hydrogen atom at 7500 K, is used for all v_r plots. Beyound $r/R_{\rm mo} = 100$, little difference is seen in the polar density with diffrent β values.

model used in the three-dimentional (3-D) adaptive mesh refinement (AMR) to inverstigate the line formation in complex geometrical configurations (see also Kurosawa, Harries, & Symington 2005). We modefied the code to handle the two-dimentional (2-D) density distribution; hence, the AMR grid is now in 2-D. It was done so in order to enable us to explore the rather large parameter space (c.f. section 2). Note that the velocity field is still in 3-D – the third component can be calculated by using the symmetry for a given value of azimutal angle. The examples of how the AMR grid for the purpose of the radiative transfer is constructed are presented in e.g. Wolf et al. (1999), Kurosawa & Hillier (2001) and Steinacker et al. (2003) .

The computation of the Hα is devided in two parts: 1. the source function calculation and 2. the observed flux/profile calulcation. In the first process, we have utilized the method by Klein & Castor (1978) (see also Rybicki & Hummer 1978; Hartmann et al. (1994)) in which the Sobolev approximation method is applied. The population of the bound states of hydrogen are assumed to be in statistical equilibrium, and the gas to be in radiative equilibrium. Our hydrogen atom model consist of 14 bound state and continuum. Readers are refer to Klein & Castor (1978) for details. (AND MORE..)

To compute the observed line profile, the Monte Calro radiative transfer method (e.g. Hillier 1991) using the Soblev escape-probabiliy can be used when I. a large velocity gradiant is present in the gas flow, and II. the intrinsic line width is negleible compared to the Doppler broadeing of the line. In our earlier models (Harries 2000; Symington et al. 2005), this method was used to compute the line profiles since the condition I and II are resonably satisfied. However, as noted and demonstrated by Muzerolle et al. (2001), even with a moderate amount of mass-accretion rate ($10^{-7}\,{\rm M_\odot\,yr^{-1}}$), Stark broadening becomes important in the optically thick Hα line. Muzerolle et al. (2001) (MORE REF HERE) also pointed out that the observed Hαprofiles from CTTS typically have the wings extending to $500\,{\rm km\,s^{-1}}$(e.g. Edwards et al. (1994); Reipurth et al. (1996)) which cannot be explained by the infall velocity of the gas along the magneosphere.

To implement the broadening meachanism, two modedifications to our previous model (Symington et al. 2005) are necessary. First, the emission and absorption profiles must be replaced by a Voigt profle which is defined as:

$$H\left(a,y\right) \equiv \frac{a}{\pi}\int_{-\infty}^{\infty}\frac{e^{-y'^2}}{\left(y-y'\right)^2+a^2}\,dy' \tag{13}$$

where $a = \Gamma/4\pi\Delta\nu_{\rm D}$, $y = \left(\nu-\nu_0\right)/\Delta\nu_{\rm D}$, and $y' = \left(\nu'-\nu_0\right)/\Delta\nu_{\rm D}$ (c.f. Mihalas 1978). ν_0 is the line centre frequency, and $\Delta\nu_{\rm D}$ is the Doppler line width of hydrogen atom (due to its thermal motion) which is given by $\Delta\nu_{\rm D} = \left(2kT/m_{\rm H}\right)^{1/2} \times \left(\nu_0/c\right)$ where $m_{\rm H}$ is the mass of a hydrogen atom. The damping constant Γ, which depends on the physical condition of the gas, is parameterised by Vernazza, Avrett, & Loeser (1973) as follows:

$$\begin{aligned}\Gamma &= C_{\rm rad} + C_{\rm vdW}\left(\frac{n_{\rm HI}}{10^{16}\,{\rm cm^{-3}}}\right)\left(\frac{T}{5000\,{\rm K}}\right)^{0.3} \\ &\quad + C_{\rm Stark}\left(\frac{n_e}{10^{12}\,{\rm cm^{-3}}}\right)^{2/3}\end{aligned} \tag{14}$$

where $n_{\rm H\,I}$ and n_e are the number density of neutral hydrogens and that of free electrons. Also, $C_{\rm rad}$, $C_{\rm vdW}$ and $C_{\rm Stark}$ are natural broadening, van der Waals broadening, and linear Stark broadening constants respectively. We simply adopt this parameterization along with the values of broadening constants for Hα from Luttermoser & Johnson (1992), i.e. $C_{\rm rad} = 6.5\times10^{-4}$ Å, $C_{\rm vdW} = 4.4\times10^{-4}$ Å and $C_{\rm Stark} = 1.17\times10^{-3}$ Å. In terms of level populations and the Voigt profile, the line opacity for the transition $i \rightarrow j$ can be written as:

$$\chi_l = \frac{\pi^{1/2}e^2}{m_e c} f_{ij} n_j \left(1-\frac{g_j n_i}{g_i n_j}\right) H\left(a,y\right) \tag{15}$$

where f_{ij}, n_i, n_j, $g_i$and g_j are the oscillator strength, the population of i-th level, the population of j-th level, the degeneracy of the i-th level, and the degeneracy of the j-th level respectively. $m_e$and e are the electron mass and charge (c.f. Mihalas 1978).

The second modefication in our model is the replacement of the method of solving the formal solution from the Monte Calro radiative transfer method with Sobolev approximation to the direct integration method. Similarly to the notation used by Muzerolle et al. (2001), we specify the cylindical coordinates $(p,\, q,\, t)$ which is the original stellar coordinate system $(\rho,\, \phi,\, z)$ rotated by the inclination of the line of sight, i.e. the t-axis coinsides with the line of sight. The observed flux (F_ν) is given by:

$$F_\nu = \frac{1}{4\pi d^2} \int_0^{p_{\max}} \int_0^{2\pi} p \, \sin q \, I_\nu \, \mathrm{d}q \, \mathrm{d}p \tag{16}$$

where d, $p_{\max}$, and I_ν are the distance to an observer, the maximum extent to the model space in the projected (rotated) plane, and the specific intensity (I_ν) in the direction on observer at the outer boundary. For a given ray along t, the specific intensity is given by:

$$I_\nu = I_0 e^{-\tau_\infty} + \int_{-\infty}^{t_0} \eta_\nu \left(t\right) \, e^{-\tau(t)} \mathrm{d}t \tag{17}$$

where I_0 and η_ν are the intensity at the boundary on the opposite to the observer and the emissivity of the stellar atmosphere/wind at a frequency ν. For a ray which intersects with the stellar core, I_0 is computed from the stellar stompshere mode of Kurucz (1979) as descibed in section 2.1, and $I_0 = 0$ otherwise. The initial position of each ray is assigned to be at the center of the surface element ($\mathrm{d}A = p \, \sin q \, \mathrm{d}q \, \mathrm{d}p$). The code excution time is proportional to $n_p \, n_q \, n_\nu$ where n_p and n_q are the number of cylindical radial and angluar points for the flux integration, and $n_\nu$is the number of frequency points. In the models presented in the next (section 4), $n_p = 180$, $n_q = 100$, and $n_\nu = 101$ are used unless specified otherwise. The linearliy spaced radial grid is used for the area where the ray intersects with magnetpshere, and the logarithmically spaced grid is used for the wind/jet and the accretion disc regions.

The optical depth τ is equation 17 is defined as:

$$\tau \left(t\right) \equiv \int_{-\infty}^{t} \chi_\nu \left(t'\right) \, \mathrm{d}t'$$

where χ_ν is the opacity of media the ray passes through. τ_∞ is the total optical depth measured from the initial ray point to the observer (or to the outer boundary closer to the observer). Initially, the optical depth segments $\mathrm{d}\tau$ are computed at the intersections of a ray with the original AMR grid in which the opacity and emissivity infomation are stored. For high opticale depth models, additional points are inserted between the original points along the ray, and η_ν are χ_ν values are interpolated to those points to ensure $\mathrm{d}\tau < 0.05$ for the all ray segments.

For a point in the magnetosphere and the wind/jet flows, the emissivity and the opacity of the media are given as:

$$\left\{ \begin{array}{lcl} a & = & b \\ c & = & d \end{array} \right. \tag{18}$$

$$\eta_\nu = \eta_{\mathrm{c}}^{\mathrm{H}} + \eta_l^{\mathrm{H}} \tag{19}$$

and

$$\chi_\nu = \chi_c^{\mathrm{H}} + \chi_l^{\mathrm{H}} + \sigma_{\mathrm{es}} \tag{20}$$

where $\eta_{\mathrm{c}}^{\mathrm{H}}$ and η_l^{H} are the continuum and line emissivity of hydrogen. χ_c^{H}, χ_l^{H}, and σ_{es} are the contiuum, line opacity (equation 15) of hydrogen, and the electron scattering opacity.

For a point in the accretion disc,

$$\eta_\nu = 0 \tag{21}$$

and

$$\chi_\nu = \kappa_{\mathrm{abs}}^{\mathrm{dust}} + \kappa_{\mathrm{sca}}^{\mathrm{dust}} \tag{22}$$

where $\kappa_{\mathrm{abs}}^{\mathrm{dust}}$ and $\kappa_{\mathrm{sca}}^{\mathrm{dust}}$ are the dust absorption, and scattering opacity which are calculated using the dust property described in section 12. For computational simplicity, we assumed that the dust emissivity is zero. Since the disc mass of CTTS are rather small ($\sim 0.1\,\mathrm{M}_\odot$) and low temperature ($<\sim 1600\,\mathrm{K}$), the continuum flux contribution at Hα wavelength is expected to be neglegible (e.g. Chiang & Goldreich 1997). The scattering flux by the accretion may become important for Hα for the edge-on ($i \sim 90^\circ$) cases in which the disc obscures the stellar surface – the main source of contiuum flux. We examine this effect later in section **??**.

The new flux integraion method are tested against the

4 RESULTS

4.1 Magnetosphere

Using the standard parameters (Table 1) for the central star and the magentosphere, we examine the dependency of Hα on the temperature ($T_{\max}$) of accretion flow and the mass accretion rate ($\dot{M}_{\mathrm{acc}}$), as similarly done by Muzerolle et al. (2001) for Hβ. The hot ring temperature is computed from the avilable kinetic energy of the free-falling gas as describe by Hartmann et al. (1994) while Muzerolle et al. (2001) used the constant hot ring temperature (8000 K) for most of their models. The accretion luminosity (L_{acc}) of models with $\dot{M}_{\mathrm{acc}} = 10^{-7}\,\mathrm{M}_\odot\,\mathrm{yr}^{-1}$ is about a half of the total luminosity (without the hot ring) of the star, and $L_{\mathrm{acc}}$is proportional to $\dot{M}_{\mathrm{acc}}$. The results are placed in Figure 3. Overall dependency on $T_{\max}$ and $\dot{M}_{\mathrm{acc}}$ are similar to that of Muzerolle et al. (2001). In general, the line strength becomes weaker as the accretion rate and the temperature become smaller. The red-shifted absorption becomes less visible for higher accretion rate and temperature models in which the flux in the damping wings become important. Figure 4 shows an example of the effect of the boradening of H alpha (with $T_{\max} = 7500\,\mathrm{K}$ and $\dot{M}_{\mathrm{acc}} = 10^{-7}\,\mathrm{M}_\odot\,\mathrm{yr}^{-1}$) due to the damping constants as described in section 3. Although the maximum flux of the model with the broadening is almost identical to that of the model with no damping constant ($\Gamma = 0$), a significant increase of the line flux in both red and blue wings of seen in the model with broadening. A weak red-shifted absorption component (which is a signiture of the magnetospherical accretion) is weakened or eliminated by the flux in broadened wing.

Table 2 shows the EW for the models shown in Figure 3. About a half of the models shown the figure agree with the observed EW values of Hα from 30 TTS presented by Alencar & Basri (2000) who found the EW of Hα ranges from $\sim$ 3 Å to $\sim$ 160 Å, and the mean to be $\sim$ 55 Å. For the lowest $\dot{M}_{\mathrm{acc}}$ models, the EW values are smaller than the minimum EW observed by Alencar & Basri (2000), and for some models the EWs are negative. Since the target selection criteria of Alencar & Basri (2000) is not stated in their paper, we can not conclude that these low $\dot{M}_{\mathrm{acc}}$models disagree with the observation. Reipurth et al. (1996), who measured the EW of 43 TTS and found similar distribution of EW values, mentioned that their EW measurements are underrepresenting real samples since the selection of the targerts are based on the strong Hα emission in Hα surveys.

The dependency of the profile on the inclination angle (i) is demonstrated in Figure 5. The model uses the same paramters

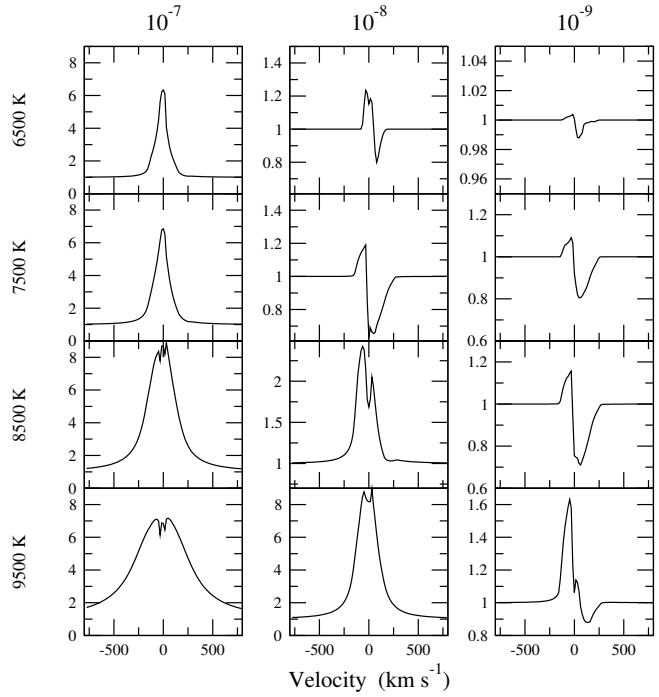

Figure 3. Hα model profiles for wide ranges of mass accretion rate ($\dot{M}$) and temperature ($T_{\rm max}$). All the profiles are computed using the parameters of the 'standard' model (Table 1) and inclination $i = 55^{\circ}$. The temperature (indicated along the vertical axis) of the model increase from the top to the bottom, and the mass accretion rate (indicated by the values in $\rm M_{\odot}\,yr^{-1}$ at the top) increases from left to right. The profiles are similar to those of Muzerolle et al. (2001), available on-line (http://cfa–www.harvard.edu/cfa/youngstars/models/magnetospheric_models.html).

as in Figure 4 (with broadening, $T_{\rm max} = 7500\,{\rm K}$ and $\dot{M}_{\rm acc} = 10^{-7}\,{\rm M_{\odot}\,yr^{-1}}$). The figure show that the peak (normalized) flux decrease as the inclination angle increases. Similarly, the equivalent width also decreases as the inclination increases. Because of the geometry of the magnsepsherical accretion (c.f. Figure 1) and of the presence of the gas with the highest velocity close to the stellar surface, the highest red-shifted line-of-sight velocity is visible only at the high incination angles. This explains the wider appearence of the profile with $i = 80^{\circ}$compared to the relatively narrow line appearence of the profile with $i = 10^{\circ}$. Although not show here, a similar depdency on the inclination angle is found for the models with different temperatures ($T_{\rm max} = 6500, 8500, 9500\,{\rm K}$).

As seen in the models of Hartmann et al. (1994) and Muzerolle et al. (2001), our models also show the blue-shifted peak and the blue-ward asymmetry caused by the occultation of the accretion flow by the equotrial disc and the stellar disc. On the hand, Alencar & Basri 2000 (see their Fig. 9) found a substential fraction of the observed Hα profiles also shows the "red-shifted" peak, and the P Cygni profiles which can not be explained by the magnetospherical accretion model alone. In addition, a recent study by Appenzeller et al. (2005) showed that the equivalent width of Hα increases as the inclination angle increases. Our model with the magnetospherical accreation flow clearly disagrees with their finding.

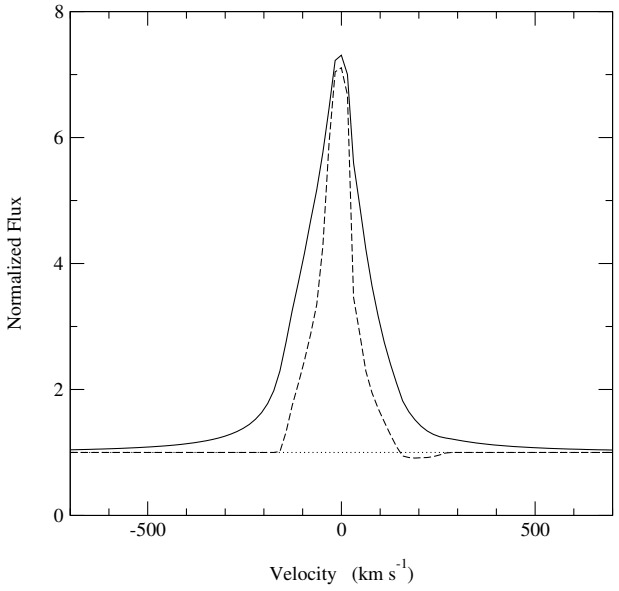

Figure 4. Effect of the line broadening for Hα. The model computed with the damping constant (Γ), described in section 3 (solid), is compared with the one with no damping constant, $\Gamma = 0$ (dashed). Both models are computed with $T_{\rm max} = 7500$ K, $i = 55^{\circ}$, and the standard parameters given in Table 1. The two models have similar peak flux levels (around $V \sim 0\ {\rm km\ s^{-1}}$), but the total flux and the EW of the line increased drastically for the model with the damping constant. The broaded wings extend to $\sim \pm 900{\rm km\ s^{-1}}$. The redshifted absorption feature (very weakly) seen in the $\Gamma = 0$ model are not seen in the model with the broadening.

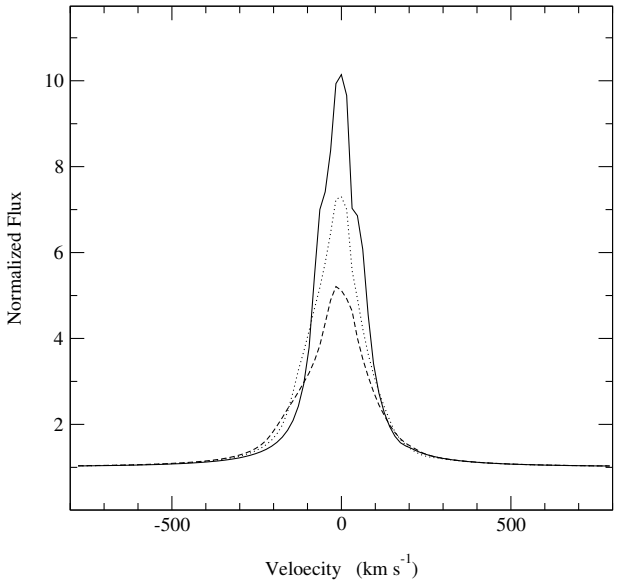

Figure 5. Dependecy of Hα profiles on inclination (i). The profiles are computed with the magneospherical accretion flow using the standard parameters given in Table 1 and $T_{\rm max} = 7500$ K. The solid, dotted, and dashed lines are for $i = 10^{\circ}$, 55°, and 80° respectively. As the inclination becomes larger, the peak flux and the equivalent width of the line becomes smaller. Similar dependency is seen in the models with $T_{\rm max} = 6500, 8500, 9500$ K (not shown here).

$T_{\rm max}$ (K)	$\dot{M}_{\rm acc}$ $(\mathrm{M}_\odot\,\mathrm{yr}^{-1})$		
	10^{-7}	10^{-8}	10^{-9}
6500	17.9	0.1	0.0
7500	25.2	−0.9	−0.5
8500	68.3	6.5	−0.7
9500	98.6	52.4	1.3

Table 2. The summary of Hα equivalent widths from the magnetospherical accretion flow models show in Figure 3.

4.2 Wind/Jet only

The basic wind model parameters introduced in section 2.3 are γ, β, v_∞, b, $\theta_{\rm wind}$, $T_{\rm wind}$ and $\dot{M}_{\rm wind}$. To minimize the number of parameters to be explored, we initially adopte $\gamma = 0.05$, $v_\infty = 200\,\mathrm{km\,s^{-1}}$ (Appenzeller et al. 2005). Futher, the extent of the wind is assumed to be close to the edge of the accretion disc, i.e. $\theta_{\rm wind} = 80^\circ$. The degree of collimination is initially chosen to be $b = 4$, i.e. the ratio of the density in polar direction to the density at the edge of the wind close to the accretion disc is about $(\cos 0^\circ / \cos 80^\circ)^4 \approx 10^3$ from equation 8. With these parameters kept constant, we examine the characterstics of Hα profiles, as a function of the wind accereation paramter β and the isothermal wind temperature $T_{\rm wind}$. Dependency on the other parameters will be discussed later in this section.

The results with the mass-loss rate $\dot{M}_{\rm wind} = 10^{-8}\,\mathrm{M}_\odot\,\mathrm{yr}^{-1}$ are shown in Figure XXX.

4.3 Magnetosphere + wind/jet

4.4 Magentosphere + disc + wind/jet

- Flux contribution by scattering of photon by disc?

4.5 Summary

5 DISCUSSION

5.1 Classification scheme proposed by Reipurth et. al (1996)

Reipurth et al. (1996) proposed the two-dimentional classification of Hα emission profiles of T Tauri stars and Herbig Ae/Be stars. Their classification scheme contains four classes (I, II, III and IV) differenciated by the ratio of the secondary-to-primary emission components in the profiles. Each classes are devided into two subclasses (B and R) which depends whether the absorption componet is on the blue or red side. Readers are refered to Fig. 4 of their paper.

- comparison with observations.
- other possible model? Better wind model?
- Any other bussiness?

6 CONCLUSIONS

We presented the detailed study of the Hα formation from the circumstealler material of classical T Tauri stars. AND MORE.

ACKNOWLEDGEMENTS

RK is supported by PPARC standard grand PPA/G/S/2001/00081.

References

Alencar S. H. P., Basri G., 2000, AJ, 119, 1881
Anders E., Grevesse N., 1989, geochim. cosmochim. acta, 53, 197
Appenzeller I., Bertout C., Stahl O., 2005, A&A, 434, 1005
Appenzeller I., Mundt R., 1989, A&AR, 1, 291
Basri G., Bertout C., 1989, ApJ, 341, 340
Bertout C., Basri G., Bouvier J., 1988, ApJ, 330, 350
Blandford R. D., Payne D. G., 1982, MNRAS, 199, 883
Burrows C. J., Stapelfeldt K. R., Watson A. M., Krist J. E., Ballester G. E., Clarke J. T., Hester J. J., Hoessel J. G., Holtzman J. A., Mould J. R., Scowen P. A., Trauger J. T. andWestphal J. A., 1996, ApJ, 473, 437
Calvet N., Basri G., Kuhi L. V., 1984, ApJ, 277, 725
Calvet N., Hartmann L., Hewett R., 1992, ApJ, 386, 229
Castor J. I., Lamers H. J. G. L. M., 1979, ApJS, 39, 481
Chiang E. I., Goldreich P., 1997, ApJ, 490, 368
Collier Cameron A., Campbell C. G., 1993, A&A, 274, 309
Cotera A. S., Whitney B. A., Young E., Wolff M. J., Wood K., Povich M., Schneider G., Rieke M., Thompson R., 2001, ApJ, 556, 958
Decampli W. M., 1981, ApJ, 244, 124
Draine B. T., Lee H. M., 1984, ApJ, 285, 89
Edwards S., Cabrit S., Strom S. E., Heyer I., Strom K. M., Anderson E., 1987, ApJ, 321, 473
Edwards S., Hartigan P., Ghandour L., Andrulis C., 1994, AJ, 108, 1056
Frank J., King A., Raine D. J., 2002, Accretion Power in Astrophysics: Third Edition. Cambridge Univ. Press, Cambridge, p. 398
Ghosh P., Pethick C. J., Lamb F. K., 1977, ApJ, 217, 578
Grevesse N., Noels A., 1993, in Origin and Evolution of the Elements, N. P., E. V.-F., M. C., eds., Cambridge Univ. Press, Cambridge, p. 15
Guenther E. W., Emerson J. P., 1996, A&A, 309, 777
Gullbring E., Hartmann L., Briceno C., Calvet N., 1998, ApJ, 492, 323
Hanner M., 1988, in NASA Conf. Pub. 3004, 22, Vol. 3004, p. 22
Harries T. J., 2000, MNRAS, 315, 722
Hartigan P., Edwards S., Ghandour L., 1995, ApJ, 452, 736
Hartmann L., Avrett E., Edwards S., 1982, ApJ, 261, 279
Hartmann L., Hewett R., Calvet N., 1994, ApJ, 426, 669
Herbig G. H., 1962, Advances in Astronomy and Astrophysics, 1, 47
Hillier D. J., 1991, A&A, 247, 455
Johns-Krull C. M., Valenti J. A., Hatzes A. P., Kanaan A., 1999, ApJ, 510, L41
Kenyon S. J., Hartmann L., 1987, ApJ, 323, 714
Kenyon S. J., Hartmann L., Hewett R., Carrasco Cruz-Gonzalez I., Recillas E., Salas L., Serrano A., Strom K. M., Strom S. E., Newton G., 1994, AJ, 107, 2153
Kim S., Martin P. G., Hendry P. D., 1994, ApJ, 422, 164
Klein R. I., Castor J. I., 1978, ApJ, 220, 902
Knigge C., Woods J. A., Drew E., 1995, MNRAS, 273, 225
Königl A., 1991, ApJ, 370, L39
Königl A., Pudritz R. E., 2000, Protostars and Planets IV, 759
Krasnopolsky R., Li Z.-Y., Blandford R. D., 2003, ApJ, 595, 631
Kuhi L. V., 1964, ApJ, 140, 1409
Kurosawa R., Harries T. J., Bate M. R., Symington N. H., 2004, MNRAS, 351, 1134
Kurosawa R., Harries T. J., Symington N. H., 2005, MNRAS, 358, 671

Kurosawa R., Hillier D. J., 2001, A&A, 379, 336
Kurucz R. L., 1979, ApJS, 40, 1
—, 1993, VizieR Online Data Catalog, 6039, 0
Kwan J., Tademaru E., 1995, ApJ, 454, 382
Luttermoser D. G., Johnson H. R., 1992, ApJ, 388, 579
Martin S. C., 1996, ApJ, 470, 537
Mathis J. S., Rumpl W., Nordsieck K. H., 1977, ApJ, 217, 425
Mihalas D., 1978, Stellar atmospheres, 2nd edn. W. H. Freeman and Co., San Francisco
Muzerolle J., Calvet N., Hartmann L., 2001, ApJ, 550, 944
Ouyed R., Pudritz R. E., 1997, ApJ, 482, 712
Pudritz R. E., Banerjee R., 2005, ArXiv Astrophysics e-prints
Ray T. P., Mundt R., Dyson J. E., Falle S. A. E. G., Raga A. C., 1996, ApJ, 468, L103+
Reipurth B., Pedrosa A., Lago M. T. V. T., 1996, A&AS, 120, 229
Rybicki G. B., Hummer D. G., 1978, ApJ, 219, 654
Shakura N. I., Sunyaev R. A., 1973, A&A, 24, 337
Shu F. H., Najita J., Ostriker E., Wilkin F., Ruden S., Lizano S., 1994, ApJ, 429, 781
Steinacker J., Henning T., Bacmann A., Semenov D., 2003, A&A, 401, 405
Symington N. H., Harries T. J., Kurosawa R., 2005, MNRAS, 356, 1489
Takami M., Bailey J., Chrysostomou A., 2003, A&A, 397, 675
Uchida Y., Shibata K., 1985, PASJ, 37, 515
Ustyugova G. V., Koldoba A. V., Romanova M. M., Chechetkin V. M., Lovelace R. V. E., 1995, ApJ, 439, L39
Vernazza J. E., Avrett E. H., Loeser R., 1973, ApJ, 184, 605
Walker C., Wood K., Lada C. J., Robitaille T., Bjorkman J. E., Whitney B., 2004, MNRAS, 351, 607
Wolf S., Henning T., Stecklum B., 1999, A&A, 349, 839
Wood K., Wolff M. J., Bjorkman J. E., Whitney B., 2002, ApJ, 564, 887